Microporous and Mesoporous Materials 158 (2012) 7–12

Contents lists available at SciVerse ScienceDirect

Microporous and Mesoporous Materials

journal homepage: www.elsevier.com/locate/micromeso

Porous silica as supports for controlled fabrication of $Au/CeO_2/SiO_2$ catalysts for CO oxidation: Influence of the silica nanostructures

Li-Hui Ren, Hui-Li Zhang, An-Hui Lu, Yan Hao, Wen-Cui Li *

State Key Laboratory of Fine Chemicals, School of Chemical Engineering, Faculty of Chemical, Environmental and Biological Science and Technology, Dalian University of Technology, Dalian 116024, PR China

ARTICLE INFO

Article history:
Received 23 December 2011
Received in revised form 11 February 2012
Accepted 4 March 2012
Available online 13 March 2012

Keywords:
Porous silica
$Au/CeO_2/SiO_2$
CO oxidation
HMS

ABSTRACT

Porous silica with different nanostructures, namely two-dimensional hexagonal SBA-15, three-dimensional cubic KIT-6 and hierarchical monolith silica (HMS), were used as supports to fabricate gold catalysts using a liquid-phase deposition–precipitation method. Pre-loading of ceria on porous silica can significantly improve the dispersion of the subsequently introduced gold nanoparticles and the catalytic activity of the final composite ($Au/CeO_2/SiO_2$) catalysts in CO oxidation. The composite catalysts were characterized by N_2 adsorption, X-ray diffraction. The results indicate that different nanostructures of silica imposed significant influence on the catalytic activity of $Au/CeO_2/SiO_2$ catalysts. Gold catalyst supported on HMS exhibited the highest activity for the conversion of CO to CO_2 with a complete conversion ($T_{100\%}$) at a temperature of 60 °C and at a space velocity of 80,000 mL g_{cat}^{-1} h^{-1}, whereas $T_{100\%}$ shifted to 120–130 °C for SBA-15 and KIT-6 supported gold catalysts.

1. Introduction

Silica materials with many excellent properties, such as high thermal stability and high surface area, are probably the mostly studies and commonly used porous solids in the field of catalysis and sorption and separation [1,2]. Nowadays, precise control over the nanostructures of silica materials by designed synthesis provides a possibility for the fabrication of model catalysts to well understand the intrinsic relation between structure and catalytic performance. The representative nanostructured silica materials include two-dimensional hexagonal SBA-15 and MCM-41, three-dimensional cubic KIT-6 and MCM-48, and hierarchically porous monolith silica (HMS). Many kinds of noble metal active species have been loaded on the surface of such structurally well-defined silica materials to fabricate model catalysts with an aim to improve the catalytic performance and understand the structure–activity relationship of nanocatalysts [2–5].

So far, only a few kinds of porous silica materials have been investigated as gold supports, though gold nanoparticles ($\leqslant$5 nm in size) exhibits extremely high low-temperature catalytic activity. That is because the highly negatively charged surface of silica under deposition–precipitation (DP) conditions (pH 6–10) causes difficulty in incorporation of anionic $Au(OH)_xCl_{4-x}^-$ complexes from $HAuCl_4$ precursor and then large gold particles generally above 10 nm will be formed. To create strong interaction between the silica and gold particles and obtain small gold nanoparticles on the silica support, ordered mesoporous silica need to be modified with amine ligands followed by loading $HAuCl_4$ and calcination [6]. Alternatively, the cationic precursor $Au(en)_2Cl_3$ (en: ethylenediamine) can be used for the immobilization of gold on the negatively charged silica surface using DP method. The resultant catalyst is active for CO oxidation even below 273 K [7]. In addition, vapor deposition instead of wet-chemistry method has also been conducted to load gold nanoparticles on the surface of silica [8,9]. To facilitate the incorporation of gold nanoparticles in a silica matrix, investigators also developed direct synthesis of Au/mesoporous SiO_2 by either mixing Au^{3+} [10–14] or gold colloids [15–18] with SiO_2 source. However, the obtained Au/mesoporous SiO_2 mostly showed limited activity. Moreover, Huang and coworkers have investigated the gold catalysts supported on inert silica matrix (Qingdao Haiyang Chemicals Co.; no detailed description about the silica structure.) modified with CoO_x [19], ZnO [20] and NaOH [21].

As known, ceria is considered as an active support for oxidation reaction. Corma et al. reported that Au deposited on nanocrystalline ceria showed two orders of magnitude in the catalytic activity relative to the Au/CeO_2 catalysts prepared by coprecipitation and by Au deposition on a regular ceria support [22]. However, the gold particles supported on pure ceria is less stable than those supported on mixed oxide supports [23]. Hence, in order to fully utilize the advantage of ceria and silica, the great interest and challenge is to prepare $Au/CeO_2/SiO_2$ three-component nanostructure [24] catalyst in a more facile way.

* Corresponding author. Tel./fax: +86 411 84986140.
E-mail address: wencuili@dlut.edu.cn (W.-C. Li).

1387-1811/$ - see front matter © 2012 Elsevier Inc. All rights reserved.
http://dx.doi.org/10.1016/j.micromeso.2012.03.010

In this paper, three kinds of mesoporous silica including two-dimensional hexagonal SBA-15, three-dimensional cubic KIT-6 and hierarchical monolith silica (HMS) were first modified with a small amount of ceria and then employed as composite supports for gold nanoparticles. The introduction of CeO_2 can improve the deposition of gold nanoparticles into porous channels of silica supports. The relation between the catalytic activity for CO oxidation reaction of the multi-component catalyst ($Au/CeO_2/SiO_2$) and nanostructure of silica was then investigated.

2. Experimental section

2.1. Catalyst preparation

The silica supports including SBA-15 [25], KIT-6 [26] and HMS [27,28] were prepared according to the literatures. An aqueous solution of $Ce(NO_3)_2{\cdot}6H_2O$ was used as the ceria precursor and impregnated into porous silica via incipient wetness impregnation. Due to the capillary force of the mesopores, the aqueous solution was sucked into the porous spaces of these porous silica supports. The samples were dried at 50 °C for 4 h and then calcined at 300 °C for 2 h in a muffle oven under air to obtain CeO_2/SBA-15, CeO_2/KIT-6 and CeO_2/HMS composites. The gold nanoparticles were deposited on the as-synthesized composites by deposition–precipitation (DP) with urea as the precipitating agent. Typically, 0.3 g composite support was added to 25 mL aqueous solution of $HAuCl_4$ and urea (molar ratio of urea: Au = 100:1). The suspension was then heated to 80 °C under vigorous stirring for 6 h. Finally the solid was filtered and washed several times with pure water. The resulting powder was dried at room temperature overnight in a vacuum desiccator. The obtained catalysts were denoted as Au/CeO_2/SBA-15, Au/CeO_2/KIT-6 and Au/CeO_2/HMS, respectively. Approximately 3 wt.% of gold and 10 wt.% of ceria were used on the silica supports.

2.2. Catalyst characterization

Powder X-ray diffraction (XRD) was performed on a Philips X' pert PRO X-ray diffractometer (Cu Kα radiation, λ = 0.154178 nm). N_2 sorption was performed at -196 °C using a Micromeritics Tri star 3000 device, following pre-treatment at 120 °C under vacuum for 4 h to remove all adsorbed species. The surface area (S_{BET}) was measured using the Brunauer–Emmett–Teller (BET) model. Pore size distribution (PSD) curves were calculated by the Barrett–Joyner–Halenda (BJH) method from the desorption branch. The position of the maximum of the PSD was used as the pore diameter (D_{max}). The total pore volume (V_{total}) was estimated from the amount adsorbed at the relative pressure of 0.99. The microstructure of the catalysts was characterized with a Hitachi HF2000 microscope equipped with a cold field emission emitter at a beam energy of 200 kV and a cooled Si (Li) energy-dispersive X-ray (EDX) spectrometer from ThermoNoran Instruments for point resolved elemental analysis. Over 18 points were tested in order to obtain statistically reliable data. The gold loading in the catalyst was analyzed by inductively coupled plasma atomic emission spectrometer (ICP-AES) on the Optima 2000DV.

2.3. Catalytic activity measurement

The activities in CO oxidation were measured using 50 mg of sieved catalyst (250–500 μm) in a gas mixture (1 vol.% CO, 20 vol.% O_2 and N_2 remainder at a flow rate of 67 mL min^{-1}, corresponding to a space velocity of 80,000 mL g_{cat}^{-1} h^{-1}). The reactant and product composition were analyzed by a GC 7890T gas chromatograph equipped with a thermal conductivity detector. Before catalytic tests, the catalysts were pretreated in a mixture of nitrogen and hydrogen (ratio 6:1 by volume) at a flow rate of 40 mL min^{-1}, at 250 °C for 2 h.

3. Results and discussion

3.1. Structure characterization of $Au/CeO_2/SiO_2$

Three silica with different structures (two-dimensional hexagonal SBA-15, three-dimensional cubic KIT-6 and hierarchically structured monolith HMS) were used to construct composite catalysts. The XRD patterns of these composite catalysts are shown in Fig. 1. The peaks at 28.6, 33.1, 47.5 and 56.3° are accordingly ascribed to the (111), (200), (220) and (311) planes of ceria. Commonly, the reflections at 38.2 and 44.3° of Au/CeO_2/SBA-15 can be assigned to metallic gold nanoparticles. The broad reflection peaks indicate that the particle sizes are small. For sample Au/CeO_2/KIT-6 and Au/CeO_2/HMS, the reflection at 2θ = 44.3° is hardly visible, and only the reflection at 38.2° is observed, indicating even smaller gold particles size on these silica supports. The estimated gold particle sizes (using the Scherrer equation) of the Au/CeO_2/HMS and Au/CeO_2/KIT-6 catalysts are ca. 2.5 nm, while Au/CeO_2/SBA-15 has larger gold nanoparticles with a size of ~5 nm. The average particle size of ceria on Au/CeO_2/HMS is ~5 nm, which is slightly larger than that (3 nm) of Au/CeO_2/KIT-6 and Au/CeO_2/SBA-15. These results were further confirmed by TEM observation of the catalysts (see Fig. 4).

The N_2 sorption isotherms and pore size distributions (PSDs) of the silica supports, CeO_2/SiO_2 composites and the corresponding $Au/CeO_2/SiO_2$ catalysts are shown in Fig. 2a–f. The calculated texture parameters of these materials are compiled in Table 1. KIT-6 and SBA-15 show type IV isotherms with a remarkable hysteresis loop over the relative pressure ranging from 0.5 to 0.7 for KIT-6, and 0.6 to 0.8 for SBA-15, indicating mesoporous characteristic. HMS shows a well-pronounced H1 type hysteresis loop above P/P_0 = 0.8 and the nitrogen uptake does not reach a plateau, indicating the existence of large pores. As seen in Fig. 2b, the PSDs exhibit a narrow pore size distribution concentrated around 5.7 nm for KIT-6 and 6.7 nm for SBA-15, while HMS has a wide PSD ranging from mesopore to macropore. After ceria was introduced, the isotherms of composite (Fig. 2c) showed a reduced adsorbed volume with no change in shape. Noticeably, sample CeO_2/SBA-15 shows a partial pore blocking effect of the mesopores, due to the introduced ceria nanoparticles. Such similar phenomenon, pore blocking effect, has been found in literature as well [29]. As shown in Table 1, the surface areas and pore volumes decreased slightly for CeO_2/HMS and CeO_2/KIT-6. The decrease in the textural parameters was mainly due to the loaded extra weight of CeO_2 in SiO_2 supports. The bulk phase densities of crystalline CeO_2 and amorphous

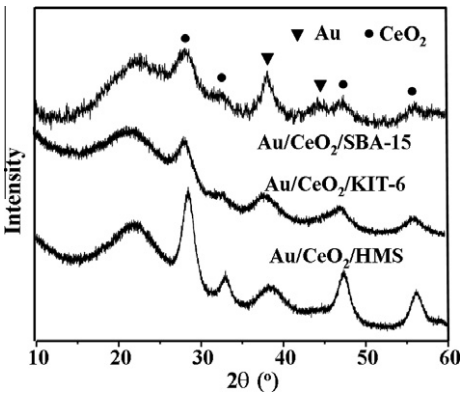

Fig. 1. XRD patterns of Au/CeO_2/KIT-6, Au/CeO_2/SBA-15 and Au/CeO_2/HMS.

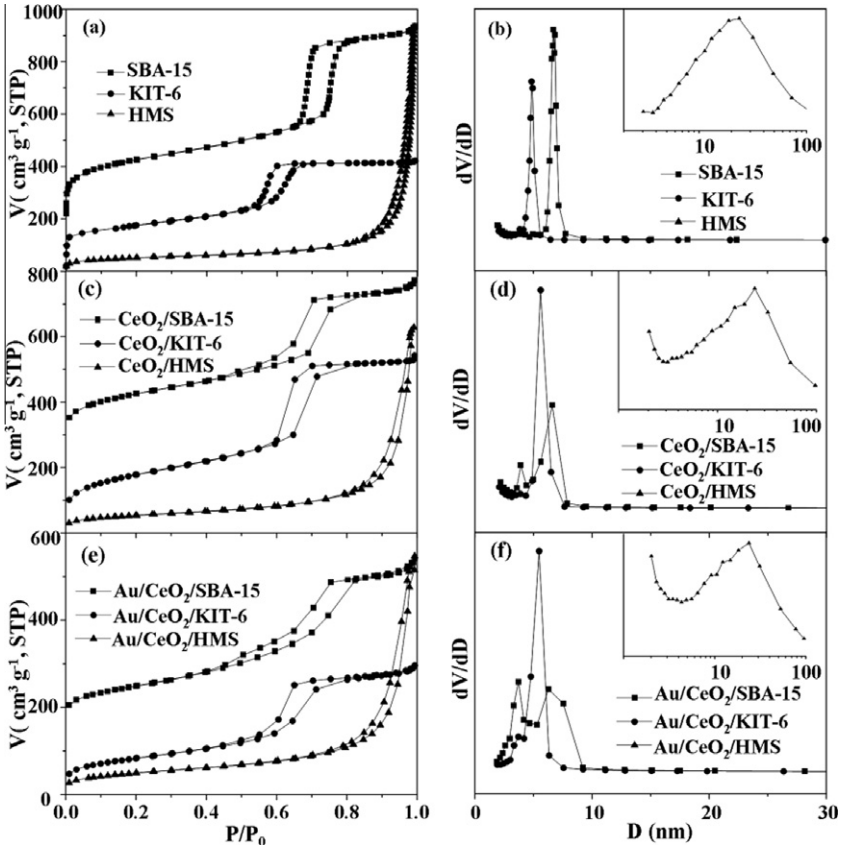

Fig. 2. Nitrogen sorption isotherms of SBA-15, KIT-6 and HMS (a), their composites (c) and catalysts (e), and their corresponding pore size distributions (b, d and f). The isotherms of SBA-15, CeO_2/SBA-15 and Au/CeO_2/SBA-15 were all offset vertically at 200 $cm^3\ g^{-1}$, respectively.

Table 1
Texture parameters of silica support before and after ceria addition and gold loading.

Sample	S_{BET} ($m^2\ g^{-1}$)	V_{total} ($cm^3\ g^{-1}$)	D_{max} (nm)
SBA-15	812	1.10	6.7
KIT-6	674	0.83	5.7
HMS	256	1.42	22.2
CeO_2/SBA-15	629	0.85	6.5
CeO_2/KIT-6	623	0.80	5.7
CeO_2/HMS	194	1.16	20.0
Au/CeO_2/SBA-15	358	0.61	3.7, 6.2
Au/CeO_2/KIT-6	300	0.46	5. 5
Au/CeO_2/HMS	179	0.85	18.8

SiO_2 are 7.6 and 2.2 g cm^{-3}, respectively [30]. The pore sizes of the silica supports and CeO_2/SiO_2 composites (Fig. 2d) are almost identical except CeO_2/SBA-15 with a small shoulder at ~3.7 nm.

As can be seen in Fig. 2e, the nitrogen sorption isotherms of the gold catalysts are also identical in shape with that of their supports. The deposition of gold nanoparticles onto their composite supports lead to significant decrease in specific surface areas and total pore volumes of KIT-6 and SBA-15. As seen in Fig. 2f, SBA-15 exhibits a bimodal pore system with sizes concentrated at 3.7 and 6.3 nm. The presence of the small mesopores with a size of 3.7 nm was attributed to the partial blocking of the mesoporous channels by the deposited gold and ceria nanoparticles. The dominant pores in Au/CeO_2/KIT-6 were retained after gold deposition. A small shoulder at ca. 3 nm in the PSD is present, which is also an indication for the pore narrowing effect caused by the deposited gold nanoparticles. However, in the case of hierarchically structured HMS, its specific surface area and total pore volume dropped gradually in the sequence of ceria and gold depositions. This, in turn, indicates that ceria and gold nanoparticles have been introduced into the pores of HMS.

3.2. Catalytic activity of Au/CeO_2/SiO_2

The Au/CeO_2/SBA-15, Au/CeO_2/KIT-6 and Au/CeO_2/HMS catalysts were tested in a CO gas mixture. For comparison and to clarify the effect of ceria, gold nanoparticles were also directly deposited on the surface of silica HMS, and the obtained Au/HMS catalyst was tested under the same reaction conditions. The activities of these catalysts for CO oxidation are displayed in Fig. 3a. The results showed that no obvious CO conversion was observed for the Au/HMS catalyst without ceria in the temperature range of 10–150 °C. The gold loading in Au/HMS was 4.05 wt.%, as determined by ICP-AES technique. Unfortunately, large gold nanoparticles with sizes of 10–60 nm were observed in the TEM image of this sample after catalytic test (Fig. 3b). The big particles are responsible for the poor catalytic activity [31,32]. In contrary, as seen in Fig. 3a, pre-introduction of ceria in silica supports would in general results in significantly improved catalytic activities. Thus the high activities of these composite catalysts are attributed to the addition of high IEP ceria on the silica surface, which results in the successful incorporation and dispersion of gold nanoparticles on the silica supports. In addition, it should be noted that the composite catalysts derived from various silica exhibit quite different catalytic performances. The calculated initial reaction rates and temperatures at 50% and 100% CO conversion are compiled in Table 2.

As seen in Table 2, The identical initial reaction rate (T = 10 °C) of Au/CeO_2/HMS, Au/CeO_2/KIT-6 and Au/CeO_2/SBA-15 were 1.74×10^{-5}, 6.07×10^{-5} and 3.94×10^{-5} $mol_{CO}\ g_{Au}^{-1}\ s^{-1}$, respectively. But when the temperature increased to 30 °C, the ordered

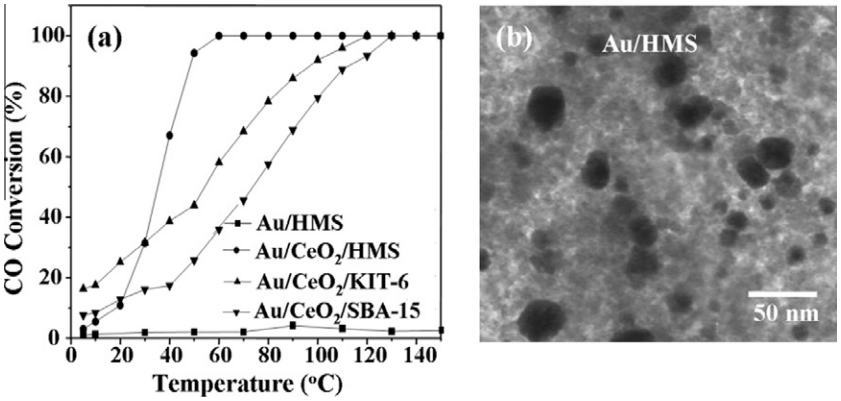

Fig. 3. (a) Catalytic curves of the $Au/CeO_2/SBA-15$, $Au/CeO_2/KIT-6$, $Au/CeO_2/HMS$ and Au/HMS composite catalysts, (b) TEM image of Au/HMS after catalysis.

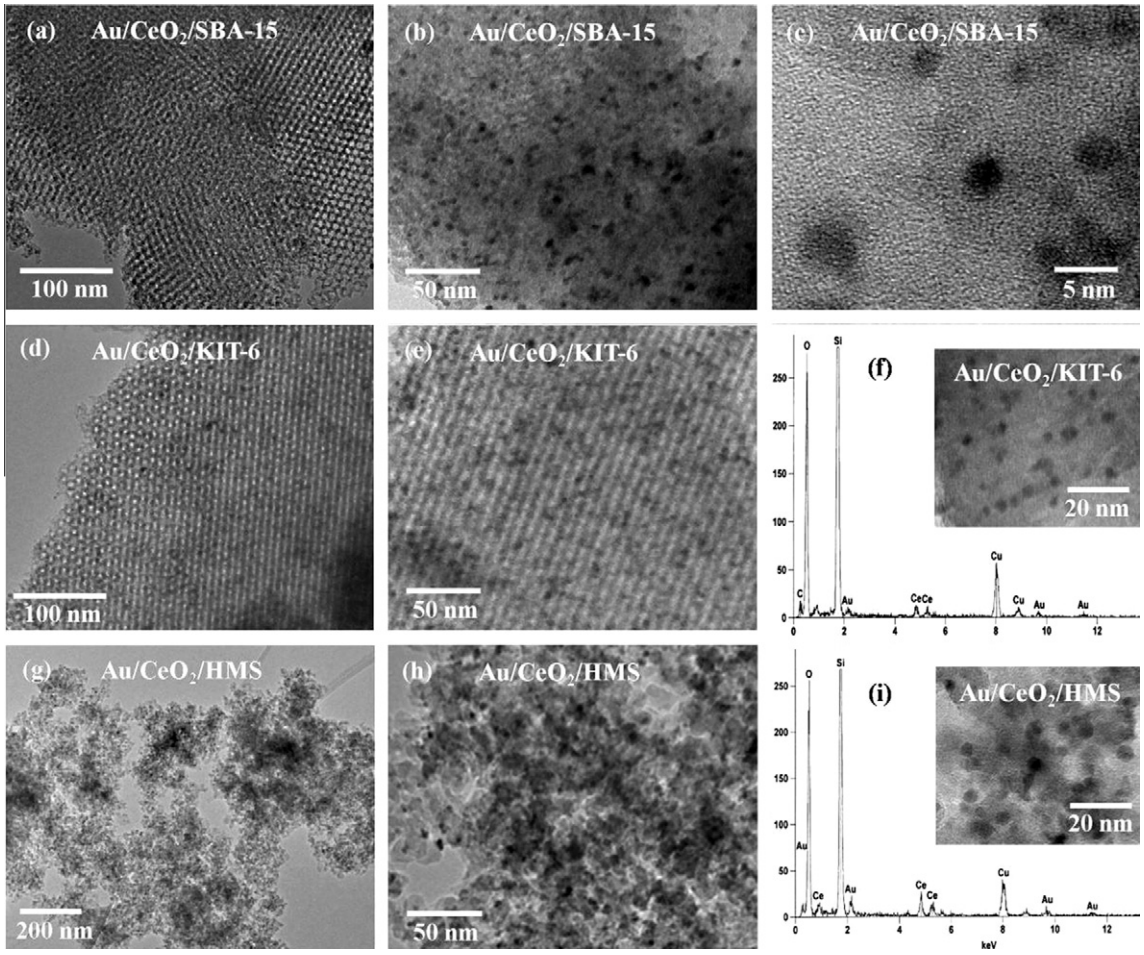

Fig. 4. TEM images of $Au/CeO_2/SBA-15$ (a–c), $Au/CeO_2/KIT-6$ (d and e), EDX results for $Au/CeO_2/KIT-6$ (f), $Au/CeO_2/HMS$ (g and h), and $Au/CeO_2/HMS$ after catalytic reaction (i).

Table 2
Particle size and content of gold and ceria, and catalytic activity of catalysts[a].

Sample	Au size (nm)	Ceria size (nm)	Au (wt.%)	Ceria (wt.%)	$T_{50\%}$ °C	$T_{100\%}$ °C	$r*10^5$ (10 °C) ($mol_{CO}\ g_{Au}^{-1}\ s^{-1}$)	$r*10^5$ (30 °C) ($mol_{CO}\ g_{Au}^{-1}\ s^{-1}$)
$Au/CeO_2/SBA-15$	5	3	2.03	12.88	70	120	3.94	7.10
$Au/CeO_2/KIT-6$	2.5	3	2.78	9.64	54	110	6.07	10.22
$Au/CeO_2/HMS$	2.5	5	3.02	9.80	34	60	1.74	9.37

[a] Sizes of Au and ceria were calculated using the Scherrer equation based on XRD patterns, the contents of Au and ceria in $Au/CeO_2/SBA-15$ were measured by ICP-AES technique, others were measured by EDX technique.

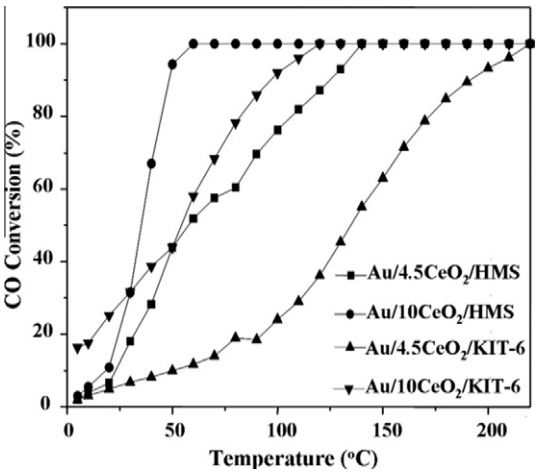

Fig. 5. Catalytic curves of CO oxidation for Au/CeO_2/KIT-6 and Au/CeO_2/HMS catalysts with different ceria amount.

of identical initial reaction rate was: Au/CeO_2/KIT-6 > Au/CeO_2/HMS > Au/CeO_2/SBA-15. With the increase of temperature, Au/CeO_2/HMS exhibited the highest activity with a complete conversion of CO to CO_2 ($T_{100\%}$) at 60 °C, while Au/CeO_2/KIT-6 and Au/CeO_2/SBA-15 catalysts had $T_{100\%}$ values of 120 and 130 °C, respectively. This suggests that the different mesostructures of the supports can exert an important influence on the catalytic performance at high conversion because the diffusion rate is becoming an important factor at high conversion [33]. HMS possesses hierarchically porous structure, which consists of relatively bigger mesopores (22.2 nm) and macropores. This kind of structure would be beneficial to mass diffusion. In contrast, the pore sizes of KIT-6 and SBA-15 are concentrated at 5.7 and 6.7 nm, respectively, without macropores. From a viewpoint of diffusion, it is acceptable that the catalytic activity of Au/CeO_2/HMS is better than that of Au/CeO_2/KIT-6 and Au/CeO_2/SBA-15. In addition, KIT-6 has three-dimensional cubic structure. Compared the SBA-15 with two-dimensional hexagonal channels, KIT-6 is obviously beneficial to a relatively fast diffusion rate. Thus the activity of Au/CeO_2/KIT-6 is slightly better than that of Au/CeO_2/SBA-15. In addition, the chemical state of gold species was mainly Au^0 (XPS data not shown here), for the catalysts were pretreated in a mixture of nitrogen and hydrogen [34,35].

3.3. TEM observation of the catalysts after CO oxidation

Furthermore, the samples were characterized by TEM and EDX analysis after the catalytic test and the results are shown in Fig. 4. Independent of the silica supports, the gold and ceria nanoparticles are homogeneously dispersed in the silica supports, and largely within the mesopores. Most particles are quite small in the range of 2–5 nm, even after the catalytic test. This is consistent with the results calculated from the XRD patterns. In order to verify whether the active components were homogeneously distributed over the entire samples, EDX analysis was performed. For each sample, more than 18 points were randomly recorded by EDX from different parts of the samples. The representative results are shown in Fig. 4f and i. It can be seen that the EDX results of the composite catalysts also show uniform and high dispersion degree of gold and ceria in the entire support. Sample Au/CeO_2/HMS possesses homogenous dispersion with average contents of 3.02 wt.% for gold and 9.80 wt.% for ceria. Correspondingly, the Au/CeO_2/KIT-6 has 2.78 wt.% of gold and 9.64 wt.% of ceria. These are almost identical to the theoretical amounts calculated before the preparation.

Obviously, ceria that was introduced into in the pores of silica supports, supplies lattice oxygen and activate oxygen for CO oxidation. Thus, all samples show enhanced catalytic activity. TEM observation confirmed that gold and ceria nanoparticles are homogenously dispersed on the silica supports, and largely within the mesopores. Furthermore, the sizes of gold and ceria nanoparticles are all in the range of 2–5 nm, as shown in the TEM images and XRD patterns. Thus the difference of CO conversion abilities should depend on the nanostructure of the support which itself has an influence on the dispersion of the gold nanoparticles. After introducing ceria nanoparticles into the mesoporous channels of SBA-15 or KIT-6, the subsequently deposited gold nanoparticles would anchor near or on these ceria nanoparticles. This may somehow cause certain blockage of the mesoporous channels, further lowering mass transfer through the channels. Differing from the SBA-15 and KIT-6, HMS has a hierarchical porosity, i.e. mesoporous framework and macropores within the silica skeleton. This structure allows a better dispersion of gold and ceria species without obvious spatial hindrance.

3.4. Influence of the ceria loading on a silica

Composite catalysts were also prepared with a reduced ceria loading of 4.5 wt.% ($Au/4.5CeO_2$/KIT-6 and $Au/4.5CeO_2$/HMS). As seen in Fig. 5, both $Au/4.5CeO_2$/KIT-6 and $Au/4.5CeO_2$/HMS catalysts with 4.5 wt.% ceria showed significantly lower CO oxidation activity compared to those catalysts with 10 wt.% of ceria. This can be attributed to the scarcity of active ceria sites in the catalysts. Remarkably, regardless of the loading of ceria, Au/CeO_2/HMS catalysts in general exhibit higher activity than KIT-6 supported gold catalysts. This strongly confirmed the important influence of the silica nanostructure on the catalytic activity of gold catalysts in CO oxidation.

4. Conclusions

We have investigated three different porous silica materials as good catalyst supports for CO oxidation. The pre-introduced ceria and the nanostructures of silica materials all have significant influence on the catalytic activity. In terms of CO oxidation activities, HMS with hierarchical porosity allows a uniform dispersion of both ceria and gold nanoparticles and a rapid mass diffusion, so as a better catalytic activity was observed compared to that of SBA-15 and KIT-6 supported gold catalysts. Hence, the great impact of the nanostructure of a support is therefore demonstrated.

Acknowledgment

The project was supported by the National Natural Science Foundation of China (No. 20973031) and the Program for New Century Excellent Talents in University of China (NCET-08-0075), and the Ph.D. Programs Foundation (20100041110017) of Ministry of Education of China. We are highly grateful to Prof. F. Schüth for helpful discussion and to Mr. B. Spliethoff for TEM measurement.

References

[1] Q. Lu, F. Gao, S. Komarneni, T.E. Mallouk, J. Am. Chem. Soc. 126 (2004) 8650–8651.
[2] H.P. Wang, C.J. Liu, Appl. Catal. B: Environ. 106 (2011) 672–680.
[3] A. Penkova, J.M. Martínez Blanes, S.A. Cruz, M.A. Centeno, K. Hadjiivanov, J.A. Odriozola, Micropor. Mesopor. Mater. 117 (2009) 530–534.
[4] L. Escamilla-Perea, R. Nava, B. Pawelec, M.G. Rosmaninho, C.L. Peza-Ledesma, J.L.G. Fierro, Appl. Catal. A: Gen. 381 (2010) 42–53.
[5] J.L. Liu, L.J. Zhu, Y. Pei, J.H. Zhuang, H. Li, H.X. Li, M.H. Qiao, K.N. Fan, Appl. Catal. A: Gen. 353 (2009) 282–287.
[6] B. Lee, Z. Ma, Z.T. Zhang, C. Park, S. Dai, Micropor. Mesopor. Mater. 122 (2009) 160–167.

[7] H.G. Zhu, C.D. Liang, W.F. Yan, S.H. Overbury, S. Dai, J. Phys. Chem. B 110 (2006) 10842–10848.
[8] G.M. Veith, A.R. Lupini, S. Rashkeev, S.J. Pennycook, D.R. Mullins, V. Schwartz, C.A. Bridges, N.J. Dudney, J. Catal. 262 (2009) 92–101.
[9] M. Okumura, S. Nakamura, S. Tsubota, T. Nakamura, M. Azuma, M. Haruta, Catal. Lett. 51 (1998) 53–58.
[10] J.C. Hu, L.F. Chen, K.K. Zhu, A. Suchopar, R. Richards, Catal. Today 122 (2007) 277–283.
[11] M. Magureanu, N.B. Mandache, J.C. Hu, R. Richards, M. Florea, V.I. Parvulescu, Appl. Catal. B: Environ. 76 (2007) 275–281.
[12] G.M. Lu, D. Ji, G. Qian, Y.X. Qi, X.L. Wang, J.S. Suo, Appl. Catal. A: Gen. 280 (2005) 175–180.
[13] B. Lee, H. Zhu, Z. Zhang, S.H. Overbury, S. Dai, Micropor. Mesopor. Mater. 70 (2004) 71–80.
[14] H. Zhu, B. Lee, S. Dai, S.H. Overbury, Langmuir 19 (2003) 3974–3980.
[15] C. Aprile, A. Abad, H. García, A. Corma, J. Mater. Chem. 15 (2005) 4408–4413.
[16] Z. Kónya, V.F. Puntes, I. Kiricsi, J. Zhu, J.W. Ager III, M.K. Ko, H. Frei, P. Alivisatos, G.A. Somorjai, Chem. Mater. 15 (2003) 1242–1248.
[17] J. Zhu, Z. Kónya, V.F. Puntes, I. Kiricsi, C.X. Miao, J.W. Ager, A.P. Alivisatos, G.A. Somorjai, Langmuir 19 (2003) 4396–4401.
[18] H.P. Lin, Y.S. Chi, J.N. Lin, C.Y. Mou, B.Z. Wan, Chem. Lett. 30 (2001) 1116–1117.
[19] K. Qian, W.X. Huang, Z.Q. Jiang, H.X. Sun, J. Catal. 248 (2007) 137–141.
[20] K. Qian, W.X. Huang, J. Fang, S.S. Lv, B. He, Z.Q. Jiang, S.Q. Wei, J. Catal. 255 (2008) 269–278.
[21] K. Qian, W.H. Zhang, H.X. Sun, J. Fang, B. He, Y.S. Ma, Z.Q. Jiang, S.Q. Wei, J.L. Yang, W.X. Huang, J. Catal. 277 (2011) 95–103.
[22] S. Carrettin, P. Concepción, A. Corma, J.M. López Nieto, V.F. Puntes, Angew. Chem. Int. Ed. 43 (2004) 2538–2540.
[23] F. Moreau, G.C. Bond, B. van der Linden, B.A.A. Silberova, M. Makkee, Appl. Catal. A: Gen. 347 (2008) 208–215.
[24] K. Qian, S.S. Lva, X.Y. Xiao, H.X. Sun, J.Q. Lu, M.F. Luo, W.X. Huang, J. Mole, Catal. A: Chem. 306 (2009) 40–47.
[25] D. Zhao, J. Feng, Q. Huo, N. Melosh, G.H. Fredrickson, B.F. Chmelka, G.D. Stucky, Science 279 (1998) 548–552.
[26] F. Kleitz, S.H. Choi, R. Ryoo, Chem. Commun. (2003) 2136–2137.
[27] J.H. Smátt, S. Schunk, Chem. Mater. 15 (2003) 2354–2361.
[28] A.H. Lu, J.H. Smátt, M. Lindén, Adv. Funct. Mater. 15 (2005) 865–871.
[29] P. Van Der Voort, P.I. Ravikovitch, K.P. De Jong, A.V. Neimark, A.H. Janssen, M. Benjelloun, E. Van Bavel, P. Cool, B.M. Weckhuysen, E.F. Vansant, Chem. Commun. (2002) 1010–1011.
[30] J. Roggenbuck, H. Schäfer, T. Tsoncheva, C. Minchev, J. Hanss, M. Tiemann, Micropor. Mesopor. Mater. 101 (2007) 335–341.
[31] M. Haruta, Gold Bull. 37 (2004) 27–36.
[32] N. Lopez, T.V.W. Janssens, B.S. Clausen, Y. Xu, M. Mavrikakis, T. Bligaard, J.K. Nørskov, J. Catal. 223 (2004) 232–235.
[33] M. Haruta, Cattech 6 (2002) 102–115.
[34] U. R Pillai, S. Deevi, Appl. Catal. A: Gen. 299 (2006) 266–273.
[35] A. Abd El-Moemen, A. Karpenko, Y. Denkwitz, R.J. Behm, J. Power Sources 190 (2009) 64–75.